JOURNAL OF GEOPHYSICAL RESEARCH, VOL. 112, D02105, doi:10.1029/2006JD007357, 2007

An ozone-modified refractive index for vertically propagating planetary waves

Terrence R. Nathan[1] and Eugene C. Cordero[2]

Received 31 March 2006; revised 4 August 2006; accepted 27 September 2006; published 20 January 2007.

[1] An ozone-modified refractive index (OMRI) is derived for vertically propagating planetary waves using a mechanistic model that couples quasigeostrophic potential vorticity and ozone volume mixing ratio. The OMRI clarifies how wave-induced heating due to ozone photochemistry, ozone transport, and Newtonian cooling (NC) combine to affect wave propagation, attenuation, and drag on the zonal mean flow. In the photochemically controlled upper stratosphere, the wave-induced ozone heating (OH) always augments the NC, whereas in the dynamically controlled lower stratosphere, the wave-induced OH may augment or reduce the NC depending on the detailed nature of the wave vertical structure and zonal mean ozone gradients. For a basic state representative of Northern Hemisphere winter, the wave-induced OH can increase the planetary wave drag by more than a factor of two in the photochemically controlled upper stratosphere and decrease it by as much as 25% in the dynamically controlled lower stratosphere. Because the zonal mean ozone distribution appears explicitly in the OMRI, the OMRI can be used as a tool for understanding how changes in stratospheric ozone due to solar variability and chemical depletion affect stratosphere-troposphere communication.

Citation: Nathan, T. R., and E. C. Cordero (2007), An ozone-modified refractive index for vertically propagating planetary waves, *J. Geophys. Res.*, *112*, D02105, doi:10.1029/2006JD007357.

1. Introduction

[2] *Charney and Drazin*'s [1961] seminal study of vertically propagating planetary waves provided one of the most oft-quoted diagnostics in dynamic meteorology: the refractive index (RI) for extratropical planetary waves propagating vertically in an inviscid, adiabatic atmosphere. Subsequent studies have obtained forms of the RI that include the effects of Newtonian cooling [e.g., *Dickinson*, 1969], Earth's spherical geometry [e.g., *Matsuno*, 1970], and longitudinal variations in the westerly current [e.g., *Nishii and Nakamura*, 2004]. Despite the qualitative success of the RI as a diagnostic measure of wave propagation and attenuation, the RI as traditionally cited is incomplete: It neglects the wave-induced heating that arises from the interactions between stratospheric ozone and planetary wavefields.

[3] Wave-induced ozone heating (OH) arises from coupled perturbations involving the wind, temperature and ozone fields. The local phasing between these fields, which depends on the ratio of advective to photochemical timescales, determines whether there is local wave damping or amplification. In the photochemically controlled upper stratosphere, a positive temperature perturbation will produce a negative ozone perturbation [*Craig and Ohring*, 1958]. The negative correlation between the temperature and ozone perturbations will enhance the thermal relaxation and thus wave damping. In the dynamically controlled lower stratosphere, the perturbation heating or cooling by the ozone field depends on the meridional and vertical transport of zonal mean ozone, where the transport is intimately coupled to the wave structure and the zonal mean ozone distribution [e.g., *Nathan and Li*, 1991]. In the middle stratosphere the situation is more complicated; the net wave-induced heating or cooling depends on both the chemistry and transport of ozone.

[4] The importance of wave-induced OH to stratospheric wave dynamics has been demonstrated for both the tropics and extratropics (see Table 1). For example, *Cordero and Nathan* [2005] have shown for the tropics that solar cycle-modulated wave-induced OH can serve as a pathway for communicating the effects of the solar cycle to the quasi-biennial oscillation. *Nathan and Li* [1991] have shown for the extratropics that the wave-induced OH can augment (reduce) the local damping rate of Newtonian cooling (NC) by as much as 50% for free, extratropical planetary waves in the upper (lower) stratosphere. However, neither of these studies nor the others cited in Table 1 have addressed the broader and more fundamental issue of how the wave-induced OH may affect the dynamical coupling between the stratosphere and troposphere. This coupling hinges in large part on the planetary waves, which are at the heart of most dynamical theories of stratosphere-troposphere communication in the extratropics.

[1] Atmospheric Science Program, Department of Land, Air and Water Resources, University of California, Davis, California, USA.
[2] Department of Meteorology, San José State University, San José, California, USA.

0148-0227/07/2006JD007357$09.00

Table 1. Selected Papers on the Effects of Wave-Induced Ozone Heating on Atmospheric Waves

Study	Model	Wave Type	Remarks
Leovy [1966]	primitive equations, f-plane	inertio-gravity wave	radiative-photochemical destabilization of inertio-gravity waves near the mesopause
Lindzen [1966]	two-layer, β-plane, quasigeostrophic	baroclinic wave	radiative-photochemical destabilization of a baroclinic zonal current to baroclinic waves in the mesosphere
Gruzdev [1985]	quasigeostrophic, vertically averaged, β-plane	free Rossby wave	ozone heating due to meridional ozone advection destabilizes planetary Rossby waves
Zhu and Holton [1986]	primitive equations, f-plane	inertio-gravity wave	radiative-photochemical damping of inertio-gravity waves in the stratosphere and lower to mid mesosphere
Nathan [1989]	quasigeostrophic, β-plane	free Rossby wave	analytical study showing how wave-induced ozone heating can alter the damping rates of free Rossby waves
Nathan and Li [1991]	quasigeostrophic, β-plane	free Rossby wave	numerical study showing how wave-induced ozone heating can alter the damping rates of free Rossby waves
Nathan et al. [1994]	quasigeostrophic, β-plane	free Rossby wave	wave-induced ozone heating destabilizes traveling waves during summer
Echols and Nathan [1996]	equatorial β-plane	Kelvin wave	wave-induced ozone heating modifies the wave fluxes that drive the semiannual oscillation
Cordero and Nathan [2000]	equatorial β-plane	Kelvin and Rossby-gravity waves	wave-induced ozone heating modifies the wave fluxes that drive the quasi-biennial oscillation
Xu et al. [2001]	primitive equations, f-plane	inertio-gravity wave	confirmed *Leovy*'s [1966] study using a more sophisticated radiative-photochemical model
Cordero and Nathan [2005]	equatorial β-plane	Kelvin and Rossby-gravity waves	wave-induced ozone heating provides a pathway for communicating the effects of solar variability to the quasi-biennial oscillation
Present study	quasigeostrophic, β-plane	forced, stationary Rossby wave	derivation of a refractive index for vertically propagating planetary waves that accounts for wave-induced ozone heating

[5] For example, several theories have been proposed to explain observational data suggesting the stratosphere may play a more important role in influencing the troposphere than previously thought [e.g., *Baldwin and Dunkerton*, 1999]. These theories include "downward control" [*Haynes et al.*, 1991], whereby a local, wave-induced anomaly in stratospheric potential vorticity induces a meridional circulation that affects the troposphere below, downward reflection of planetary waves originating in the troposphere [*Perlwitz and Harnik*, 2003], and local, wave mean flow interaction, which produces downward propagating, zonal mean wind anomalies [*Plumb and Semeniuk*, 2003]. Although these theories appear distinct, they have a common, unifying element: They all have as their basis, either explicitly or implicitly, wave propagation and attenuation. Yet none of these theories include the effects of wave-induced OH on planetary wave propagation and attenuation, an omission that could affect wave reflection as well as the wave drag on the zonal mean flow. Thus omitting wave-induced OH in describing planetary wave dynamics could result in an incomplete description of troposphere-stratosphere communication.

[6] As observational evidence continues to grow showing changes in the amount and distribution of stratospheric ozone [*World Meteorological Organization* (*WMO*), 2002], it has become increasingly important to understand its interaction with the planetary waves, an interaction that for the most part remains poorly understood. As we will show, a fundamental measure of this interaction, one which embodies in a single diagnostic the effects of the background flow and the wave-induced ozone heating on wave propagation and attenuation, is an ozone-modified refractive index (OMRI). The real part of the OMRI describes the wave propagation and the imaginary part describes the wave attenuation, the latter being a measure of the planetary wave drag on the zonal mean flow. The derivation and analysis of this OMRI will serve two primary purposes: first, it will provide insight into the effects of OH on vertical wave propagation and attenuation, wave properties that are intimately connected to stratosphere-troposphere communication; second, it will provide a conceptual framework for providing insight into how stratospheric ozone variations arising from anthropogenic processes (e.g., chlorofluorocarbons) and natural processes (e.g., 11-year solar cycle) may impact the wave driving of the stratosphere, thus highlighting a potentially important pathway for communicating stratospheric ozone changes to the climate system.

[7] The paper is organized as follows. Section 2 describes the linear, mechanistic model that accounts for wave-induced OH and NC. Section 3 describes the derivation of the OMRI and considers several limiting cases to highlight the physics that connects the OH to the planetary wave dynamics. Section 4 presents the numerical results for the OMRI, wave vertical structure, and wave drag on the zonal mean flow. The results are discussed in light of natural and human caused changes in stratospheric ozone in section 5, and the concluding remarks are given in section 6.

2. Model and Governing Equations

[8] We consider a stratified atmosphere on a periodic β-plane centered at 45°N in which the quasigeostrophic

Table 2. List of Symbols

Symbol	Definition
t, x, y, $z = -Hln(p/p_o)$	time and distances in the eastward, northward, and vertical directions
$p(z)$, p_o	pressure, reference pressure at the ground
$\rho = \rho_o \exp(-z/H)$	basic state density, ρ_0 = surface density, H = 7 km is the density scale height
f_o, β	planetary vorticity and planetary vorticity gradient evaluated at $\theta = 45°$ latitude
$N^2(z)$, $\sigma = N^2/f_o^2$	Brünt Väisäla frequency, $\sigma = N^2/f_o^2$ (nondimensional stratification parameter)
$\kappa = R/C_p$	R is the gas constant and C_p the specific heat at constant pressure
$\overline{u}(z)$, $\overline{T}(y, z)$, $\overline{\gamma}(y, z)$	basic state zonal wind, temperature and ozone fields
$\phi(x, y, z, t)$	perturbation geostrophic stream function
$\Phi(x, y, z, t) = f_0\phi(x, y, z, t)$	geopotential height
$w(x, y, z, t)$	perturbation vertical wind component
$\gamma(x, y, z, t)$	perturbation ozone volume mixing ratio
$\Gamma_j(z; \overline{\gamma}, \overline{T}, \vartheta)$ $(j = 1, 2)$	radiative-photochemical coefficients in temperature equation
$\Gamma_T(z)$	Newtonian cooling coefficient
$\xi_j(z; \overline{\gamma}, \overline{T}, \vartheta)$ $(j = 1, 2, T)$	radiative-photochemical coefficients in ozone continuity equation
ϑ	solar zenith angle
$h(x, y)$	topographic height

flow is linearized about a steady, zonally averaged basic state that is in radiative-photochemical equilibrium. The basic state is assumed to vary only with height in order to more easily isolate the physics associated with the coupling between the stratospheric ozone and planetary wavefields. The linear response of this model atmosphere to ozone heating (OH) and Newtonian cooling (NC) is described by coupled equations for the quasigeostrophic potential vorticity and ozone volume mixing ratio. These equations take the following form in log-pressure coordinates [*Nathan and Li*, 1991]:

$$\left(\frac{\partial}{\partial t}+\overline{u}\frac{\partial}{\partial x}\right)\left[\nabla^2\phi+\frac{1}{\rho}\frac{\partial}{\partial z}\left(\frac{\rho}{\sigma}\frac{\partial\phi}{\partial z}\right)\right]+\beta_e\frac{\partial\phi}{\partial x}=\frac{1}{\rho}\frac{\kappa}{f_0H}\frac{\partial}{\partial z}\left(\frac{\rho}{\sigma}Q\right), \tag{1}$$

$$\left(\frac{\partial}{\partial t}+\overline{u}\frac{\partial}{\partial x}\right)\gamma+\frac{\partial\phi}{\partial x}\frac{\partial\overline{\gamma}}{\partial y}+w\frac{\partial\overline{\gamma}}{\partial z}=S, \tag{2}$$

where

$$\beta_e=\beta-\frac{1}{\rho}\frac{d}{dz}\left(\frac{\rho}{\sigma}\frac{d\overline{u}(z)}{dz}\right) \tag{3}$$

is the basic state potential vorticity gradient. The perturbation potential vorticity, $q(x, y, z, t)$, diabatic heating rate per unit mass, $Q(x, y, z, t)$, net ozone production and destruction, $S(x, y, z, t)$, and vertical motion, $w(x, y, z, t)$, are given by

$$q=\nabla^2\phi+\frac{1}{\rho}\frac{\partial}{\partial z}\left(\frac{\rho}{\sigma}\frac{\partial\phi}{\partial z}\right), \tag{4}$$

$$Q=\Gamma_1\gamma-\Gamma_2\int_z^\infty\frac{\rho(z')}{\rho_0}\gamma dz'-f_0\frac{H}{\kappa}\Gamma_T\frac{\partial\phi}{\partial z}, \tag{5}$$

$$S=-\xi_1\gamma+\xi_2\int_z^\infty\frac{\rho(z')}{\rho_0}\gamma dz'-\frac{f_0H}{R}\xi_T\frac{\partial\phi}{\partial z}, \tag{6}$$

$$w=\frac{1}{f_0\sigma}\left[-\left(\frac{\partial}{\partial t}+\overline{u}\frac{\partial}{\partial x}\right)\frac{\partial\phi}{\partial z}+\frac{d\overline{u}}{dz}\frac{\partial\phi}{\partial x}+\frac{\kappa}{H}\frac{Q}{f_0}\right]. \tag{7}$$

[9] The integral appearing in (5) and (6) can be written, after repeated integration by parts, in a form that will ease the analytical derivation of the OMRI to be presented in section 3, i.e.,

$$\chi=\int_z^\infty\frac{\rho(z')}{\rho_0}\gamma dz'=\sum_{n=0}^{\infty}H^{n+1}\frac{\partial^n\gamma}{\partial z^n}\exp(-z/H). \tag{8}$$

[10] In the above equations $\gamma(x, y, z, t)$ is the ozone volume mixing ratio and $\phi(x, y, z, t)$ is the geostrophic stream function, where $\partial\phi/\partial z$ is proportional to temperature. The remaining symbols appearing in (1)–(7) are listed in Table 2.

[11] The radiative-photochemical parameterizations appearing in (5) and (6) depend only on height and are described in detail in *Nathan and Li* [1991]. Briefly, the terms on the right-hand side (rhs) of (5) together represent the net diabatic heating rate per unit mass. The first term is the local ozone heating rate and the second term is the heating rate arising from variations in perturbation column ozone above a given level (termed the shielding effect). The radiative-photochemical coefficients $\Gamma_1(z; \overline{\gamma}, \overline{T}, \vartheta)$ and $\Gamma_2(z; \overline{\gamma}, \overline{T}, \vartheta)$ depend on the basic state distributions of ozone, $\overline{\gamma}(y, z)$ and temperature, $\overline{T}(y, z)$ as well as the solar zenith angle, ϑ. The last term in (5) represents longwave radiational cooling, which we model as Newtonian cooling (NC) based on the parameterization of *Dickinson* [1973].

[12] The terms on the rhs of (6), which represent the net ozone production and destruction, are derived from the *Chapman* [1930] reactions, wherein we have accounted for the catalytic destruction of odd oxygen by hydrogen and nitrogen chemistry by adjusting the pure oxygen destruction rate as in the work by *Hartmann* [1978]. Consistent with the heating rate coefficients, the ozone production and destruction coefficients $\xi_1(z; \overline{\gamma}, \overline{T}, \vartheta)$, $\xi_2(z; \overline{\gamma}, \overline{T}, \vartheta)$ and $\xi_T(z; \overline{\gamma}, \overline{T}, \vartheta)$ depend on the basic state distributions of ozone and temperature and solar zenith angle.

[13] At the lower boundary we impose a bottom topography $h(x, y)$, which produces the vertical velocity $w = \overline{u}\partial h/\partial x$. Insertion of this expression for w into (7) yields the lower boundary condition at $z = 0$. For the analytical solutions presented in section 3, a radiation condition is applied at the upper boundary; that is, we require that the vertical energy flux be bounded and directed upward as $z \rightarrow \infty$. For the numerical calculations presented in section 4, the upper boundary is placed at 100 km, which our calculations show to be sufficiently high to prevent spurious wave reflections that may contaminate the solutions.

3. Ozone-Modified Refractive Index

[14] The derivation of the local, ozone-modified refractive index (OMRI) hinges on the assumption that the basic state fields for wind, temperature and ozone are slowly varying in the vertical. Tacitly, the zonal mean ozone gradients, $\overline{\gamma}_y$ and $\overline{\gamma}_z$, are also assumed to be slowly varying. Under the assumption that the basic state fields are slowly varying, we approximate the shielding integral (8) as $\chi \approx H\gamma\exp(-z/H)$ and introduce the "slowly varying" vertical coordinate $\zeta = \varepsilon z$, for which $\partial/\partial z \rightarrow \partial/\partial z + \varepsilon\partial/\partial\zeta$, where $\varepsilon \ll 1$ is nondimensional. Because the coefficients in (5)–(7) vary only with height, solutions for the stream function and ozone fields are sought in the form

$$[\varphi(x,y,z,t,\zeta;\varepsilon),\gamma(x,y,z,t,\zeta;\varepsilon)] = [\hat{\varphi}(\zeta;\varepsilon),\hat{\gamma}(\zeta;\varepsilon)] \cdot \exp(z/2H)\exp(i(kx+ly-\omega t)) + c.c., \quad (9)$$

where k and l are the zonal and meridional wave numbers, ω is a fixed frequency, and c.c. denotes the complex conjugate of the preceding term. The slowly varying vertical structures for the density weighted stream function and ozone fields are chosen WKB in form [*Bender and Orszag*, 1978]:

$$[\hat{\varphi}(\zeta),\hat{\gamma}(\zeta)] = [A(\zeta),B(\zeta)]\exp\left[i\left(\frac{1}{\varepsilon}\int_0^\zeta m(\zeta')d\zeta'\right)\right]. \quad (10)$$

[15] Insertion of (9)–(10) into (1)–(2) yields, to leading order, the OMRI,

$$m(\zeta) = m_0(\zeta)\left(\frac{m_2(\zeta) \pm (1+m_3(\zeta))^{1/2}}{1-m_1(\zeta)}\right), \quad (11)$$

where m represents the local (complex) vertical wave number. The $O(\varepsilon)$ balance yields the stream function and ozone amplitudes:

$$A(\zeta) = c_0\exp\left[\int_0^\zeta a(\zeta')d\zeta'\right], \quad (12a)$$

$$B(\zeta) = b(\zeta)A(\zeta), \quad (12b)$$

where c_0 is a constant; $a(\zeta)$ and $b(\zeta)$ depend on the background distributions of wind, temperature and ozone and are defined in Appendix A. Although the focus in this study is on the analysis of the OMRI (11), it is important to note that an analysis of the amplitude (12a) is needed to address the effects of wave-induced OH heating on planetary wave reflection. In particular, an altitude where $A(\zeta) \rightarrow \infty$ corresponds to a reflecting surface. If such a surface exists, then the solution assumed for the disturbance field (10) would have to be modified to include both upward and downward propagating disturbances. The ratio of the upward to downward propagating wave amplitudes would measure the planetary wave reflection. Although one can in principle derive an expression for the reflection coefficient that shows explicitly how the stratospheric wave-induced OH can affect the planetary wave structure in the troposphere, the problem poses several technical difficulties, not the least of which is dealing with the possibility of complex turning surfaces [see, e.g., *Boyd*, 1998, section 4.3]. For this reason, we hereafter consider background flows that are void of reflecting surfaces and defer the reflection problem to a future study. Our focus for the remainder of this study will be on the wave physics described by the OMRI (11).

[16] The terms in the OMRI (11) are defined as

$$m_0^2 = \sigma\left(\frac{\beta k}{(\overline{u}k-\omega)} - \left(k^2+l^2\right)\right) - \frac{1}{4H^2}, \quad (13a)$$

$$m_1 = \tilde{\Gamma}_1\left((1-i\tau_T)\frac{(\overline{u}k-\omega)}{f_0\sigma}\frac{\partial\overline{\gamma}}{\partial z} + i\frac{f_0H}{R}\xi_T\right) + i\tau_T, \quad (13b)$$

$$m_2 = \frac{1}{m_0}\left(i\tilde{\Gamma}_1\frac{k}{2}\frac{\partial\overline{\gamma}}{\partial y} + i\frac{m_1}{2H}\right), \quad (13c)$$

$$m_3 = -m_1\left(1+\frac{1}{4H^2m_0^2}\right) - \tilde{\Gamma}_1\frac{k}{H}\frac{(1-m_1)}{m_0^2}\frac{\partial\overline{\gamma}}{\partial y} - \frac{m_2}{m_0}\frac{1}{H} - m_2^2, \quad (13d)$$

where $\tilde{\Gamma}_1$, which is proportional to the ozone heating coefficient, and τ_T, which is the ratio of advective to Newtonian cooling timescales, are defined in Appendix B. The $m_j(\zeta)$ $(j = 1–3)$ arise from NC and OH and are nondimensional. Because observations show the large-scale stratospheric circulation to be dominated by forced stationary waves [e.g., *Randel*, 1987], we hereafter set $\omega = 0$.

[17] The real part of m controls the propagation of the wave and the imaginary part of m controls its attenuation. The latter also controls the wave drag on the zonal mean flow, measured by the divergence of Eliassen-Palm (EP) flux. In the quasigeostrophic framework the divergence of EP flux is equivalent to the meridional flux of potential vorticity, i.e., $\rho^{-1}\nabla \bullet \mathbf{F} = \overline{vq}$, where F is the EP flux vector [*Andrews et al.*, 1987]. Because our background flow varies only in the vertical, the potential vorticity flux is due solely

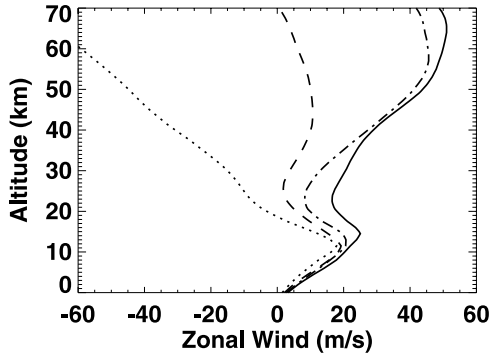

Figure 1. Vertical variations of the basic state zonal wind at 45°N for January (solid), March (dashed), July (dotted) and September (dash-dotted) based on observational data compiled by *Fleming et al.* [1988].

to the vertical convergence of northward heat flux. Using (10)–(12), we obtain, to leading order:

$$\overline{vq} = -2m_i m_r k \frac{|A|^2}{\sigma} \exp\left(\frac{z}{H} - 2\int_0^{\zeta} \frac{m_i}{\varepsilon} d\zeta'\right). \qquad (14)$$

In accordance with the *Charney and Drazin* [1961] nonacceleration theorem, in the absence of wave damping, for which $|A| = \sqrt{\sigma/m_r}$ (see Appendix A) and $m_i = 0$, the potential vorticity flux vanishes. The extent to which the wave-induced OH violates the nonacceleration theorem is measured by the wave attenuation, i.e., the imaginary part of the OMRI.

[18] Before considering the detailed properties of the OMRI and its effect on the wave structure and zonal mean flow, we begin with a discussion of some of its broader properties. To provide guidance for the following analyses, the zonal mean wind and ozone gradients are displayed in Figures 1 and 2 based on observational data at 45°N for January, March, July, and September, which have been chosen to represent their respective seasons.

[19] Consider first the simplest case of adiabatic flow for which $m = m_r = \pm m_0$. This is the RI first obtained by *Charney and Drazin* [1961]. To ensure that the wave energy propagates vertically away from its assumed tropospheric source region, causality demands that the vertical wave energy flux be directed upward as $z \to \infty$. This requires that the positive solution be chosen for m_0. The turning level, defined by $m_0 = 0$, separates wave evanescent regions ($m_0^2 < 0$) from wave propagation regions ($m_0^2 > 0$). The range of zonal mean wind for which there is vertical propagation is given by $0 < \overline{u} < \overline{u}_c$, where the critical trapping velocity is $\overline{u}_c \equiv \beta/[k^2 + l^2 + (f_0^2/N^2)/4H^2]$. Thus vertical propagation requires westerly winds that are not too strong, with the window for propagation closing with increasing horizontal wave numbers. This is consistent with observations; planetary waves are mostly confined to the troposphere during summer when the stratospheric winds are easterly and propagate into the stratosphere during the other seasons when the stratospheric winds are westerly [e.g., *Randel*, 1987].

[20] The extent to which the OH and NC affect the OMRI depends on the strength of the zonal mean wind, $\overline{u}$. Equations (13a)–(13d), with $\omega = 0$, show that NC and the OH due to vertical ozone advection are both proportional to $\overline{u}^{-1}$, whereas the OH due to meridional ozone advection is proportional to $\overline{u}^{-2}$. Thus if $\overline{u}$ is relatively weak, as it is around the time of the equinoxes, the diabatic effects due to OH and NC are relatively strong. However, in the vicinity of a zero wind line ($\overline{u} \to 0$), the meridional ozone advection is the dominant diabatic process and thus would play an important role in the absorption and reflection properties of the wave. Zero wind lines exist in the lower stratosphere during the extratropical summer (see Figure 1) and throughout the year in the subtropics. Although the effects of zero wind lines on wave-induced OH is beyond the scope of the present study, we note that *Nathan et al.* [1994] have demonstrated that the extratropical zero wind line causes the OH to more than offset the damping due to NC, leading to the amplification of traveling waves during summer. To what extent *Nathan et al.*'s [1994] results carry over to the stationary waves or to the subtropical zero wind line remains unclear and will be considered in a sequel to this study.

[21] The OMRI (11) makes clear the nonlinear coupling of the radiative-photochemical processes. This nonlinear coupling is evidenced by the dependence of m_3 on m_2^2, which contains terms such as $\overline{\gamma}_z\Gamma_1\Gamma_T$, $\overline{\gamma}_y\Gamma_1\Gamma_T$, $\overline{\gamma}_z^2\Gamma_1^2$ etc. We

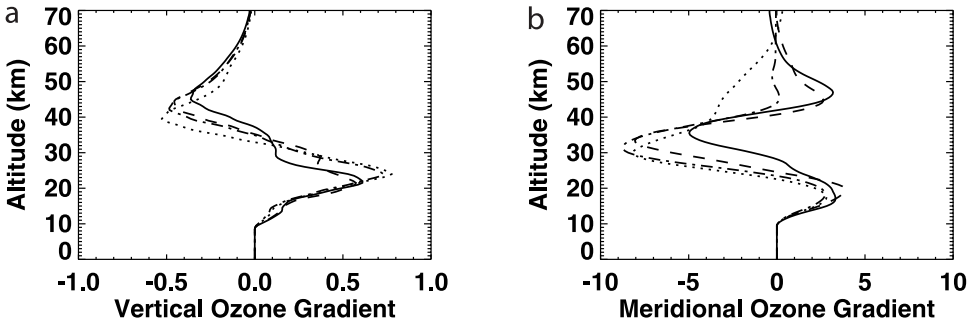

Figure 2. Vertical variations of (a) the vertical ozone gradient, $\overline{\gamma}_z$, and (b) the meridional ozone gradient, $\overline{\gamma}_y$, for January (solid), March (dashed), July (dotted) and September (dash-dotted). The zonal mean ozone mixing ratios are based on *Keating and Young* [1985] between about 10 and 90 km and HALOE data [*Brühl et al.*, 1996] between about 90 and 100 km. To obtain the ozone gradients at 45°N, the values at 40°N and 50°N were averaged.

have carried out several test calculations using climatological basic states and found these nonlinear terms to be generally small. However, these nonlinear radiative-photochemical coupling terms will likely have an important effect on the OMRI during stratospheric warming events, i.e., when the departures of the zonal mean ozone and temperature are far from their climatological values. During the warming event of January 1980, for example, *Randel* [1993] has shown that that the zonal mean ozone changed by as much as 15% (4%) in the extratropical upper (lower) stratosphere, while the temperature increased by about 10–20 K over much of the extratropical stratosphere.

[22] To understand the roles of NC and OH in controlling m, it is convenient to divide the stratosphere into three regions based on whether the ozone is under dynamical or photochemical control. The three regions are the dynamically controlled lower stratosphere, corresponding to $S \approx 0$ in (2), the middle stratosphere or transition region where dynamical and photochemical processes are of comparable importance, and the photochemically controlled upper stratosphere, corresponding to S large in (2). We consider below the dynamically and photochemically controlled regions of the stratosphere, which are amenable to further analytical analysis.

[23] In the dynamically controlled lower stratosphere ozone is approximately conserved. Thus we set ξ_1, ξ_2 and ξ_T equal to zero in (13). In addition, we choose the positive root in (11), which corresponds to upward energy propagation, i.e., $\rho\overline{w\varphi} > 0$. Further, when the NC and OH are assumed small in (13) such that $\Gamma_T \rightarrow \varepsilon\Gamma_T$ and $\tilde{\Gamma}_1 \rightarrow \varepsilon\tilde{\Gamma}_1$, an assumption that is valid except near critical levels ($\overline{u} \rightarrow 0$) or turning surfaces ($m_0 \rightarrow 0$), the real and imaginary parts of the OMRI take the following forms:

$$m_r(\zeta) \approx m_0 + \varepsilon\frac{1}{2H}\frac{1}{\overline{u}k}\left(-\underbrace{\Gamma_T}_{NC} + \underbrace{\frac{\kappa}{f_0 H\sigma}\Gamma_1\frac{\partial\overline{\gamma}}{\partial z}}_{\substack{\text{Vertical ozone}\\ \text{advection}}}\right) + \underbrace{\varepsilon M_r\left(\frac{\kappa}{2fH_0}\right)\frac{\Gamma_1}{\overline{u}^2 k}\frac{\partial\overline{\gamma}}{\partial y}}_{\substack{\text{Meridional ozone}\\ \text{advection}}}, \tag{15a}$$

$$m_i(\zeta) \approx -\varepsilon m_0\frac{M_i}{\overline{u}k}\left(-\underbrace{\Gamma_T}_{NC} + \underbrace{\frac{\kappa}{f_0 H\sigma}\Gamma_1\frac{\partial\overline{\gamma}}{\partial z}}_{\substack{\text{Vertical ozone}\\ \text{advection}}}\right) + \varepsilon\underbrace{\left(\frac{\kappa}{2f_0 H^2}\right)\frac{\Gamma_1}{m_0\overline{u}^2 k}\frac{\partial\overline{\gamma}}{\partial y}}_{\substack{\text{Meridional Ozone}\\ \text{Advection}}}, \tag{15b}$$

where the coefficients $M_r = (1-1/2Hm_0)$ and $M_i = (2-1/(2Hm_0)^2)$ are positive except near a turning surface ($m_0 \rightarrow 0$), a region where the approximations (15a) and (15b) become invalid.

[24] In the lower stratosphere, the vertical wave propagation, measured by m_r, and the vertical wave attenuation (amplification), measured by $m_i > 0$ (<0), are modulated by two wave-induced OH effects: vertical ozone advection (VOA) and meridional ozone advection (MOA). These effects become increasingly important as the zonal mean wind or zonal wave number decreases. To obtain qualitative understanding of how the terms in (15) combine to affect the vertical phasing and local wave amplitude, we assume that m is locally constant and consider the leading order approximation to the stream function amplitude, which from (10) can be written as

$$\hat{\varphi}(\zeta) \sim \exp\left(-\frac{m_i}{\varepsilon}\zeta\right)\cos\left(\frac{m_r}{\varepsilon}\zeta\right). \tag{16}$$

Thus $m_i > 0$ and $m_r > 0$ correspond to a damped, vertically propagating wave. If there is an ozone-induced increase in both m_i and m_r, for example, the local maximum in wave amplitude decreases and shifts downward.

[25] Equation (15a) shows that NC alone yields $m_r < m_0$ and $m_i \propto \tau_T > 0$. This case was first considered by *Dickinson* [1969], who showed that the ratio of advective to Newtonian cooling timescales, measured by τ_T, becomes relatively large near the equinoxes; consequently, the planetary wave amplitudes are reduced at that time, in qualitative agreement with observations.

[26] The diabatic heating due to zonal mean ozone advection by the planetary wave may augment or oppose the NC depending on the altitude. Between about 10 km and 37 km, where $\overline{\gamma}_z > 0$ (see Figure 2a), the diabatic heating due to VOA opposes the NC. Between about 10 km and 29 km, where $\overline{\gamma}_y > 0$ (see Figure 2b), the heating due to MOA augments the NC. Thus in the lowest part of the stratosphere the VOA and MOA are offsetting, though the MOA will tend to dominate over the VOA when the zonal mean winds are westerly and sufficiently weak. Between about 29 km and 40 km the heating due to MOA and VOA combine to oppose the NC.

[27] In the photochemically controlled upper stratosphere, the zonal mean ozone gradients become small (see Figure 2), whereas the ratio of advective to photochemical timescales becomes large (see Figure 3). If the NC and OH are again assumed small in (11), then the real and imaginary parts of the OMRI take the following forms:

$$m_r \approx m_0 - \varepsilon\frac{M_r}{\overline{u}k}\left(\underbrace{\Gamma_T}_{NC} + \underbrace{\frac{\kappa}{R}\Gamma_1\frac{\xi_T}{\xi_1}}_{\substack{\text{Photochemical}\\ \text{Cooling}}}\right), \tag{17a}$$

$$m_i \approx \varepsilon m_0\frac{M_i}{\overline{u}k}\left(\underbrace{\Gamma_T}_{NC} + \underbrace{\frac{\kappa}{f_0 H}\Gamma_1\frac{\xi_T}{\xi_1}}_{\substack{\text{Photochemical}\\ \text{Cooling}}}\right). \tag{17b}$$

In the upper stratosphere, photochemically accelerated cooling (PAC) combines with NC to always enhance the thermal damping. The enhanced thermal damping reduces the vertical wave propagation ($m_r < m_0$) and increases the vertical wave attenuation ($m_i > 0$).

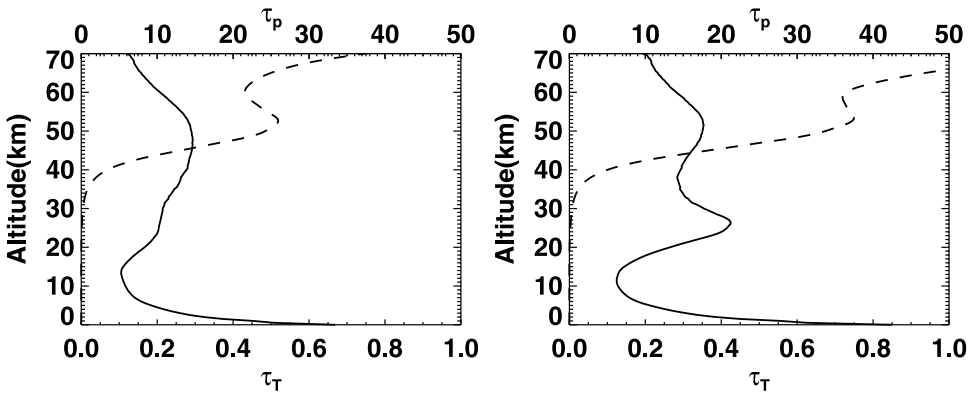

Figure 3. Vertical distribution of the ratio of advective to Newtonian cooling timescales, τ_T (solid line), and the ratio of advective to photochemical timescales, τ_p (dashed line), for the (left) January and (right) March zonal mean wind distributions. τ_T and τ_p are defined in Appendix B. The zonal wave number is one ($n = 1$).

[28] The effect of PAC on the wave damping can also be inferred from the phasing between the ozone and temperature fields. If we consider the steady form of (2) and neglect ozone advection and shielding we obtain $\gamma \sim -(\xi_T/\xi_1)\varphi_z$. Thus in the photochemically controlled upper stratosphere the ozone and temperature fields are 180° out of phase. Consequently, from (5), the (local) wave-induced OH and NC act in the same sense: Temperature perturbations always act to bring the wave back to thermodynamic equilibrium.

4. OMRI and Wave Vertical Structure: Numerical Results

[29] The effects of OH and NC on the OMRI and stationary wave vertical structure have been determined numerically for zonal waves one and two using the climatological basic states shown in Figure 1. Because the planetary waves are mostly trapped in the troposphere during July when the stratospheric zonal winds are easterly and strongly attenuated during September when the stratospheric zonal winds are westerly and weak, the results for these months are not presented. We instead focus on the results for January, with the results for March presented for comparison. Unless stated otherwise, the results given below are based on the following parameter setting: $n = 1$ (quantized zonal wave number), where $k = n/a_e\cos\theta$; $\theta = 45°$ (latitude); $a_e = 6.36 \times 10^6$ km (Earth's radius); $H = 7$ km (scale height); $l = 0$ (meridional wave number).

4.1. Ozone Modified Refractive Index (OMRI)

[30] Figure 4 shows the effects of the wave-induced OH on the vertical variation of the real and imaginary parts of the refractive index based on (11). With or without OH m_r is positive, corresponding to both positive northward heat flux and positive vertical energy flux [*Andrews et al.*, 1987, section 4.5]. The OH has essentially no effect on m_r below ~40 km. Between about 40 km and 52 km, where VOA, MOA and PAC each augment the NC, m_r is reduced by ~10%. Similar results are obtained for the spring basic state.

[31] Figure 4 shows that with or without OH m_i is positive, corresponding to wave attenuation. For the winter basic state, in the lower part of the stratosphere (~15 km < z < ~20 km), numerical tests based on (11) show that MOA dominates over VOA, the net effect being about a 5% enhancement of the wave attenuation in that region. Between ~22 km and ~34 km, VOA, MOA, and PAC are offsetting; thus in this region the OH has little effect on the wave attenuation. Above ~35 km the damping due to PAC quickly dominates the wave-induced OH, so much so that by ~40 km the wave attenuation, measured by m_i, has increased by ~75%.

[32] The vertical distributions of the OMRI for winter and spring are qualitatively similar. In the upper stratosphere the PAC dominates the wave-induced OH and augments the NC, whereas in the lower stratosphere the ozone advection dominates and may augment or diminish the NC depending on the wave vertical structure and distribution of zonal mean ozone. Differences between the winter and spring OMRI are due to differences in solar zenith angle and vertical distributions of wind, temperature and ozone. Calculations show, however, that the seasonal differences in the vertical wind distribution have the most important effect on the wave-induced OH.

4.2. Wave Vertical Structure

[33] The assumption that the background state is slowly varying is relaxed in this section by solving (1)–(7) directly using numerical methods. Solutions for the dependent variables and topography are chosen of the form

$$(\phi, w, \gamma) = \left[\hat{\phi}(z), \hat{w}(z), \hat{\gamma}(z)\right] \exp[z/2H + i(kx + ly)] + \text{c.c.}, \tag{18a}$$

$$h(x,y) = h_k \exp[i(kx + ly)] + c.c., \tag{18b}$$

where $\hat{\phi}(z)$, $\hat{w}(z)$, and $\hat{\gamma}(z)$ are the density weighted vertical structures for the stream function, vertical velocity and ozone fields. The stream function is related to the geopotential by $\phi(z) = f_0^{-1}\Phi(z)$. The topographic height h_k is chosen consistent with observations (see Appendix C). Equations (18a)–(18b) are substituted into (1)–(7) and then solved numerically using the procedure described in Appendix C. For all of the calculations, the upper boundary

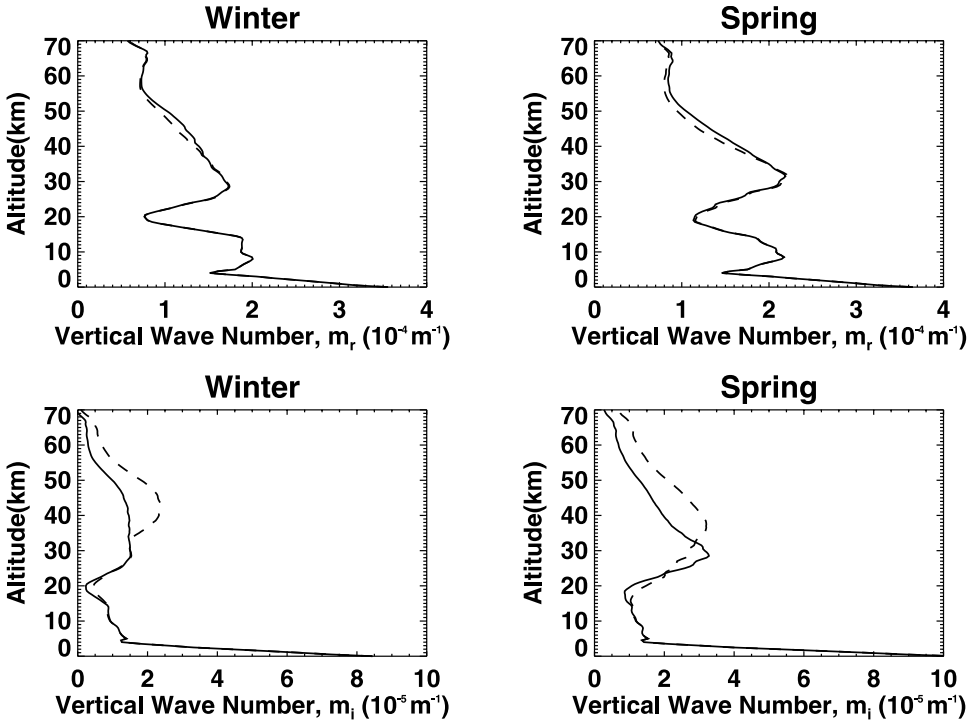

Figure 4. Vertical variation of (top) m_r and (bottom) m_i for Newtonian cooling alone (solid line) and Newtonian cooling and ozone heating combined (dotted line) for the January (winter) and March (spring) basic states. The zonal wave number is one (n = 1).

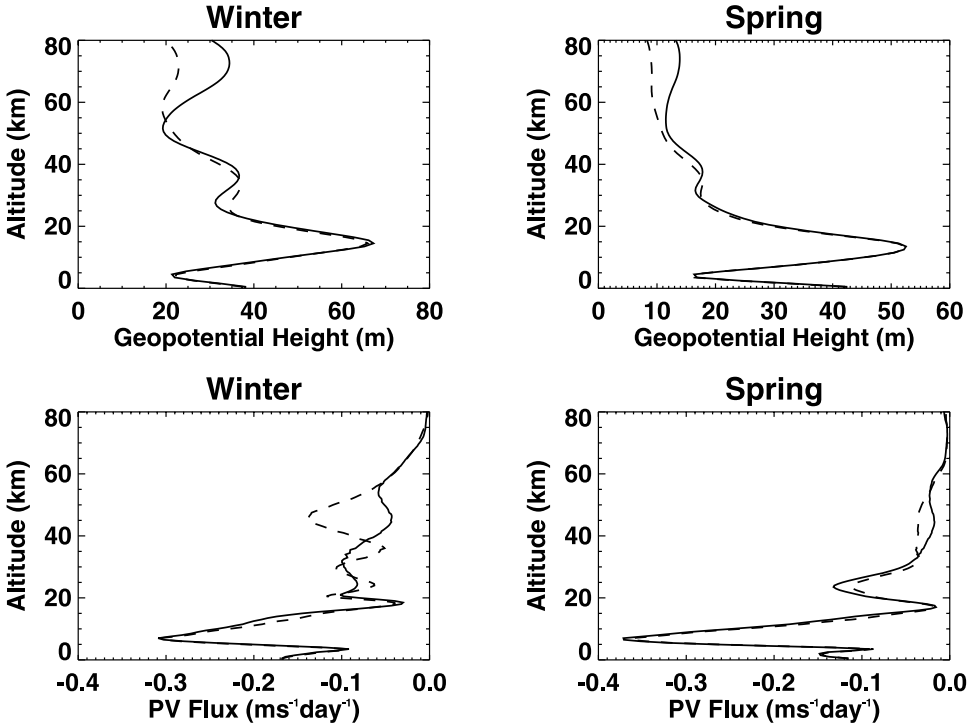

Figure 5. Vertical variation of wave vertical structure for Newtonian cooling alone (solid line) and Newtonian cooling and ozone heating combined (dotted line) for the January (winter) and March (spring) basic states. The zonal wave number is one (n = 1). Shown are the modulus of (top) geopotential height, $|\hat{\phi}(z)|$, and (bottom) potential vorticity flux, $\overline{vq}$.

is placed at 100 km, though for clarity the figures are only shown to 80 km.

4.3. Results

[34] Figure 5 shows, for the January and March basic states, the modulus of the density weighted geopotential height and the potential vorticity flux for NC alone (solid lines) and NC and OH combined (dotted lines). For the January basic state above 10 km, the geopotential height is characterized by three local maxima and two local minima. Numerical tests show that near the local minimum at ~25 km the vertical and meridional ozone advections oppose the NC and dominate over the PAC. The net effect is to lower the local minimum in geopotential height by ~1–2 km and increase it by ~10%. In the vicinity of the local maximum near ~35 km, ozone advection continues to oppose the NC and dominate over the PAC. The net effect is to lower the local maximum in geopotential height by ~4 km and increase its amplitude by ~1–2%. These ozone induced changes are consistent with equation (16); that is, a reduction in the NC due to OH will cause the peak amplitude to increase in magnitude and shift downward. Above ~55 km the PAC becomes increasingly effective and strongly damps the geopotential height. At ~60 km the PAC reduces the local maximum in geopotential height by ~40%.

[35] The effects of the wave-induced OH on the planetary wave drag, measured by the potential vorticity flux, are shown in Figure 5 (bottom left) for the January basic state. In the dynamically controlled lower stratosphere near ~25 km, the wave-induced OH reduces the wave drag by ~25%. In the region near 40 km, where ozone transitions from dynamical to photochemical control, the wave-induced heating reduces the wave drag by ~40%. Above ~40 km where the PAC augments the NC the wave drag increases by a factor of two. These results are in qualitative agreement with the OMRI (see section 3 and Figure 4) and are similar to those obtained for the March basic state (see Figure 5, bottom right).

5. Discussion

[36] Ground-based and satellite data show that stratospheric ozone varies over a broad range of space and timescales [*WMO*, 2002]. Over the past thirty years or so, two ozone signals stand out. One signal is attributed to quasi-decadal variability (QDV) in solar irradiance, termed the 11-year solar cycle, and the other to complex interactions involving changes in halogen source gasses, greenhouse gas concentrations, and volcanic aerosol loading. Although these decadal changes in ozone are relatively well documented, the pathways by which they can affect climate are not. The wave-induced ozone heating examined here is one such pathway, a pathway that communicates changes in stratospheric ozone to the zonal mean circulation via the planetary waves. The physics underlying this pathway is made clear by the ozone-modified refractive index (OMRI). To illustrate how the OMRI provides a more complete description of the connection between variations in stratospheric ozone and climate, consider the 11-year solar cycle.

[37] The 11-year solar cycle is among the natural processes associated with modulating stratospheric ozone [e.g., *Hood*, 2004]. Global climate models have shown that QDV in solar irradiance and stratospheric ozone together produce QDV in the model circulations. This QDV variability is linked in part to changes in the refractive index of the planetary waves [e.g., *Balachandran et al.*, 1999; *Shindell et al.*, 1999; *Matthes et al.*, 2004]. The linkage between the 11-year solar cycle and RI cited in these studies as well as others hinges on the following: Variations in solar spectral irradiance at primarily ultraviolet wavelengths produce variations in the photochemical production of ozone in the stratosphere. In turn, these variations in ozone produce variations in radiative heating and temperature. The corresponding meridional changes in temperature produce, via thermal wind balance, changes in the spatial distribution and strength of the zonal mean winds. The solar-induced changes in zonal mean temperature and wind produce changes in the RI of the planetary waves, measured by m_0 in this study, resulting in changes in planetary wave activity. However, as we have shown here, this traditional way of linking the solar cycle to the RI is incomplete: It neglects the effects of wave-induced OH on planetary wave activity. Moreover, because the wave-induced OH depends nonlinearly on the zonal mean wind (see (17), for example), which itself is a function of the solar-modulated ozone distribution, the wave-induced OH provides a nonlinear pathway for amplifying the effects of the 11-year cycle in solar irradiance.

[38] The OMRI highlights the direct connection between the distribution of stratospheric ozone and the planetary waves. This connection is evident in observations, though not fully understood. For example, *Fusco and Salby* [1999] have attributed the observed extratropical decline in column ozone during the 1980s to two effects: a decline in the upwelling of planetary wave activity from the troposphere into the stratosphere and chemical depletion of ozone due to elevated levels of halocarbons. However, their multiple regression analysis is unable to distinguish between the contributions of ozone photochemistry and ozone transport to the wave-induced OH, shown here to have an important impact on the vertical distribution of planetary wave drag. Because the wave-induced OH is sensitive to the coupling between the wave structure and zonal mean ozone distribution in the lower stratosphere (compare, for example, the wave drag for January and March in Figure 5), identifying the relative contributions of chemical depletion, stratospheric cooling due to increases in greenhouse gases, and changes in upwelling of planetary waves to the observed trend in ozone may be particularly difficult.

6. Concluding Remarks

[39] The refractive index (RI) is a fundamental measure of wave propagation and attenuation, wave properties that are at the heart of stratosphere-troposphere communication. Here we have employed a mechanistic model to derive an expression for an ozone-modified refractive index (OMRI) that accounts for the wave-induced heating due to coupling between the stratospheric ozone and planetary wavefields. The OMRI provides a conceptual framework for understanding how changes in the distribution and abundance of stratospheric ozone may impact planetary wave propagation, attenuation and drag on the zonal mean flow. The OMRI shows that ozone-induced changes in these planetary

wave properties occur in two ways: (1) via ozone-induced changes in the zonal mean wind and temperature fields and (2) via wave-induced OH. This latter OH effect has been overlooked in previous studies examining the role of the planetary waves in stratosphere-troposphere communication and climate.

[40] The OMRI clarifies how ozone photochemistry, wave-ozone advection and NC combine to affect planetary wave dynamics. In the photochemically controlled upper stratosphere, the wave-induced OH strongly augments the thermal damping due to NC, whereas in the dynamically controlled lower stratosphere, the wave-induced OH can augment or oppose the NC depending on the wave vertical structure and local mean ozone gradients. Using vertical distributions of wind, temperature and ozone that are consistent with Northern Hemisphere winter, we have shown that the wave-induced OH can increase the wave drag on the zonal mean flow by nearly a factor of two in the photochemically controlled upper stratosphere and decrease it by as much as 25% in the dynamically controlled lower stratosphere. Although the wave-induced OH effects are much smaller in the lower stratosphere than in the upper stratosphere, it is conceivable that in a more realistic model or for different background flows, the wave-induced OH may become more effective in altering the wave structure in the lower stratosphere.

[41] Owing to the importance of the wave-induced OH to the RI of the planetary waves, it is important to revisit those theories that rely on wave propagation and attenuation to communicate signals between the stratosphere and troposphere. As discussed in the Introduction, such theories include "downward control," local wave mean flow interaction, and the downward reflection of vertically propagating planetary waves.

[42] Modeling studies that neglect the wave-induced OH are omitting a potentially important pathway for communicating stratospheric ozone changes, both natural and human-caused, to the climate system. For the coupled chemistry-climate models that incorporate the effects of wave-induced OH, the OMRI provides a means for understanding the complicated feedbacks between stratospheric ozone and the planetary waves. The OMRI may in fact be used as a framework for designing experiments that can better isolate the potential impacts of changes in stratospheric ozone on planetary wave activity. Such experiments would aid in predicting future ozone levels [*WMO*, 2002] and understanding and predicting future climate change [*Intergovernmental Panel on Climate Change*, 2001].

[43] In this mechanistic study we have restricted our attention to vertical propagation of the planetary waves. In reality the waves generally propagate upward and then equatorward, eventually reaching the subtropical zero wind line. Studies have shown that the fate of the waves, which may manifest as reflection, absorption or a combination of both, depends crucially on the amount of mechanical damping [e.g., *Salby et al.*, 1990]. Radiative-photochemical damping will likely play a similar role, one which inhibits eddy mixing and prevents homogenization of potential vorticity. We have shown that wave-induced OH may locally dominate over NC as $\overline{u} \rightarrow 0$, which means the net radiative-photochemical damping in the vicinity of the zero wind line may be more important to planetary wave breaking and eddy mixing than previously thought. Thus extending this study to propagation in the meridional height plane is of particular interest.

[44] Other important extensions of this work include examining the sensitivity of the planetary wave response to OH for various background distributions of wind, temperature and ozone, as well as determining to what extent the changes in the distribution of stratospheric ozone may impact the downward reflection of vertically propagating planetary waves. These problems, which are currently under study, are central to providing a more complete understanding of how anthropogenic and natural changes in the stratosphere's ozone distribution may impact surface climate.

Appendix A: Stream Function and Ozone Amplitudes

[45] The WKB analysis yields for the ozone-modified stream function amplitude

$$A(\zeta) = c_0 \exp\left[\int_0^{\zeta} a(\zeta')d\zeta'\right], \tag{A1}$$

where c_0 is a constant that can be obtained from the lower boundary condition and

$$a(\zeta) = \frac{L_0 + R_0}{1 + R_1}, \tag{A2}$$

where

$$L_0 = \left[\frac{1}{2\sigma}\frac{d\sigma}{d\zeta} - \frac{1}{2m}\frac{dm}{d\zeta}\right] + i\left[-\frac{1}{4Hm\sigma}\frac{d\sigma}{d\zeta} + \frac{1}{2H(\overline{u}k-\omega)m}\frac{d\overline{u}}{d\zeta}\right], \tag{A3}$$

$$R_0 = \frac{\kappa}{f_0 H}\left[\frac{d}{d\zeta}\left(\frac{\Gamma_1}{\sigma}b\right) + \frac{k\Gamma_1}{f_0\sigma^2 H(\overline{u}k-\omega)}\frac{d\overline{u}}{d\zeta}\frac{\partial\overline{\gamma}}{\partial z}\right] \cdot \left[-\frac{2m}{\sigma}(\overline{u}k-\omega)\right]^{-1}, \tag{A4}$$

$$R_1 = \left[-\frac{\kappa\Gamma_1}{f_0 H\sigma}b + \frac{\kappa(1-i\tau_T)D\Gamma_1}{f_0^2\sigma H}\frac{\partial\overline{\gamma}}{\partial z} + i\frac{2m}{\sigma}\Gamma_T + i\frac{D\xi_T}{(\overline{u}k-\omega)}\right]\left[-\frac{2m}{\sigma}(\overline{u}k-\omega)\right]^{-1}, \tag{A5}$$

$$D(\zeta) = \left(-i(\overline{u}k-\omega) + \xi_1 + \frac{\kappa\Gamma_1}{f_0^2 H\sigma}\frac{\partial\overline{\gamma}}{\partial z}\right) \cdot \left((\overline{u}k-\omega)^2 + \xi_T - \frac{R\Gamma_T}{f_0^2 H\sigma}\frac{\partial\overline{\gamma}}{\partial z}\right)^{-1}. \tag{A6}$$

[46] The ozone and stream function amplitudes are related by $B(\zeta) = b(\zeta)A(\zeta)$, where

$$b(\zeta) = D\left[-ik\frac{\partial\overline{\gamma}}{\partial y} + \left(\frac{ik\overline{u}}{f_0\sigma}\frac{\partial\overline{\gamma}}{\partial z} - \frac{f_0 H}{R}\left(\xi_T - \frac{R\Gamma_T}{f_0^2 H\sigma}\frac{\partial\overline{\gamma}}{\partial z}\right)\right) \cdot \left(im + \frac{1}{2H}\right)\right]. \tag{A7}$$

[47] For the special case of adiabatic flow, for which $R_0 = 0$ and $R_1 = 0$, the stream function amplitude becomes

$$A(\zeta) = \sqrt{\frac{\sigma}{m}}\exp\left(i\int_0^\zeta \theta(\zeta')d\zeta'\right), \tag{A8}$$

where the phase is given by

$$\theta(\zeta) = -\frac{1}{4Hm}\frac{1}{\sigma}\frac{d\sigma}{d\zeta} + \frac{1}{2H}\frac{1}{(\overline{u}k - \omega)}\frac{1}{m}\frac{d\overline{u}}{d\zeta}. \tag{A9}$$

Appendix B: Coefficients in Equations (13a)–(13d)

[48]

$$\tilde{\Gamma}_1 = -i\frac{\kappa}{f_0 H}\left(\frac{\Gamma_1 - H\Gamma_2\exp(-\varepsilon^{-1}\zeta)}{(\overline{u}k - \omega)^2}\right)\frac{1 + i\hat{\Gamma}}{1 + \hat{\Gamma}^2}, \tag{B1a}$$

$$\hat{\Gamma} = \tau_p + \left(\frac{\kappa}{f_0^2 H\sigma}\right)\Gamma_1\frac{\partial\overline{\gamma}}{\partial z}, \tag{B1b}$$

$$\tau_T(\zeta) = \frac{\Gamma_T}{(\overline{u}k - \omega)} = \frac{NC\ time\ scale}{advective\ time\ scale}, \tag{B2a}$$

$$\tau_p(\zeta) = \frac{(\xi_1 - H\xi_2\exp(-\varepsilon^{-1}\zeta))}{(\overline{u}k - \omega)} = \frac{photochemical\ time\ scale}{advective\ time\ scale}, \tag{B2b}$$

where τ_T and τ_p are nondimensional timescales.

Appendix C: Numerical Procedure

[49] Substitution of (18) into (1)–(8), evaluating the integral in the shielding effect using the trapezoidal rule, and using second-order finite differences on staggered uniform grid in which $\hat{\phi}(z)$, $\hat{w}(z)$, and $\hat{\gamma}(z)$ are evaluated at odd and even levels, respectively, results in a set of algebraic equations that were cast in the discrete form, $\mathbf{AX} = \mathbf{B}$, where $\mathbf{A}$ is the coefficient matrix and $\mathbf{B}$ is the forcing vector. $\mathbf{B}$ only has one element corresponding to the forcing produced by topography at the lower boundary, which was obtained by averaging *Peixoto et al.*'s [1964] topographic height data in 5° intervals between 30°N and 60°N for the first two zonal modes: $h_1 = 468$ m and $h_2 = 519$ m. A Gaussian elimination routine was used to solve for the solution vector $\mathbf{X}$. To ensure that the solutions were physically relevant, i.e., void of spurious reflections from the upper boundary, we numerically solved the forced problem using several different values for the grid spacing, Δz, and several different heights for the upper boundary. We have found that $\Delta z = 0.5$ km was sufficient for resolving the wave structures and that $\hat{\phi}(z) = 0$ at 100 km was sufficient for avoiding spurious reflections from the upper boundary.

[50] **Acknowledgments.** The authors thank the anonymous reviewers for their constructive comments on the manuscript. The authors also thank Daniel Hodyss for several insightful discussions regarding this work. Support for this work was provided in part by NASA's Living with a Star, Targeted Research and Technology Program, grant LWS04-0025-0108 (T. Nathan and E. Cordero), and NSF's Faculty Early Career Development (CAREER) Program, grant ATM-0449996 (E. Cordero).

References

Andrews, D. G., J. R. Holton, and C. B. Leovy (1987), *Middle Atmosphere Dynamics*, 489 pp., Elsevier, New York.

Balachandran, N. K., D. Rind, P. Lonergan, and D. T. Shindell (1999), Effects of solar cycle variability on the lower stratosphere and the troposphere, *J. Geophys. Res.*, *104*, 27,321–27,339.

Baldwin, M. P., and T. J. Dunkerton (1999), Propagation of the arctic oscillation from the stratosphere to the troposphere, *J. Geophys. Res.*, *104*, 30,937–30,946.

Bender, C. M., and S. A. Orszag (1978), *Advanced Mathematical Methods for Scientists and Engineers*, 553 pp., McGraw Hill, New York.

Boyd, J. P. (1998), *Weakly Nonlocal Solitary Waves and Beyond-all-Orders Asymptotics*, 590 pp., Springer, New York.

Brühl, C., et al. (1996), HALOE ozone channel validation, *J. Geophys. Res.*, *101*, 10,217–10,240.

Chapman, S. (1930), On ozone and atomic oxygen in the upper atmosphere, *Philos. Mag.*, *10*, 369–383.

Charney, J., and P. Drazin (1961), Propagation of planetary scale disturbances from the lower into the upper atmosphere, *J. Geophys. Res.*, *66*, 83–109.

Cordero, E. C., and T. R. Nathan (2000), The influence of wave- and zonal mean-ozone feedbacks on the quasi-biennial oscillation, *J. Atmos. Sci.*, *57*, 3426–3442.

Cordero, E. C., and T. R. Nathan (2005), A new pathway for communicating the 11-year solar cycle to the QBO, *Geophys. Res. Lett.*, *32*(18), L18805, doi:10.1029/2005GL023696.

Craig, R. A., and G. Ohring (1958), The temperature dependence of ozone radiational heating in the vicinity of the mesopeak, *J. Met.*, *15*, 59–62.

Dickinson, R. E. (1969), Vertical propagation of planetary Rossby waves through an atmosphere with Newtonian cooling, *J. Geophys. Res.*, *74*, 929–938.

Dickinson, R. E. (1973), A method of parameterization of infrared cooling between altitudes of 30 km and 70 km, *J. Geophys. Res.*, *78*, 4451–4457.

Echols, R., and T. R. Nathan (1996), Effects of ozone heating on forced equatorial Kelvin waves, *J. Atmos. Sci.*, *53*, 263–275.

Fleming, E. L., S. Chandra, M. R. Shoeberl, and J. J. Barnett (1988), Monthly mean global climatology of temperature, wind, geopotential height and pressure for 0–120 km, *NASA Tech. Memo.*, *100697*, 85 pp.

Fusco, A. C., and M. L. Salby (1999), Interannual variations of total ozone and their relationship to variations of planetary wave activity, *J. Clim.*, *12*, 1619–1629.

Gruzdev, A. N. (1985), Effects of ozone heating on the dynamics of planetary waves, *Izv. Russ. Acad. Sci. Atmos. Oceanic Phys., Engl. Transl.*, *21*, 873–880.

Hartmann, D. L. (1978), A note concerning the effect of varying extinction on radiative-photochemical relaxation, *J. Atmos. Sci.*, *35*, 1125–1130.

Haynes, P. H., C. J. Marks, M. E. McIntyre, T. G. Shepard, and K. P. Shine (1991), On the "downward control" of extratropical diabatic circulations by eddy-induced mean zonal forces, *J. Atmos. Sci.*, *48*, 651–678.

Hood, L. (2004), Effects of solar UV variability on the stratosphere, in *Solar Variability and Its Effects on Climate*, Geophys. Monogr. Ser., vol. 141, edited by J. M. Pap and P. Fox, pp. 283–303, AGU, Washington, D. C.

Intergovernmental Panel on Climate Change (2001), *Climate Change 2001: The Scientific Basis. Contribution of Working Group 1 to the Third Assessment Report*, edited by J. T. Houghton et al., 881 pp., Cambridge Univ. Press, New York.

Keating, G. M., and D. F. Young (1985), Interim reference ozone models for the middle atmosphere, *Middle Atmosphere Program, Handbook for*

MAP, vol. 6, edited by K. Labitzke et al., 318 pp., Univ. of Ill., Champaign-Urbana.

Leovy, C. B. (1966), Photochemical destabilization of gravity waves near the mesopause, *J. Atmos. Sci.*, *23*, 223–232.

Lindzen, R. S. (1966), Radiative and photochemical processes in mesospheric dynamics: Part IV, Stability of a zonal vortex at mid-latitudes to baroclinic waves, *J. Atmos. Sci.*, *23*, 350–359.

Matsuno, T. (1970), Vertical propagation of stationary planetary waves in the winter Northern Hemisphere, *J. Atmos. Sci.*, *27*, 871–883.

Matthes, K., U. Langematz, L. L. Gray, K. Kodera, and K. Labitzke (2004), Improved 11-year solar signal in the Freie Universität Berlin Climate Middle Atmosphere Model, *J. Geophys. Res.*, *109*, D06101, doi:10.1029/2003JD004012.

Nathan, T. R. (1989), On the role of ozone in the stability of Rossby normal modes, *J. Atmos. Sci.*, *46*, 2094–2100.

Nathan, T. R., and L. Li (1991), Linear stability of free planetary waves in the presence of radiative-photochemical feedbacks, *J. Atmos. Sci.*, *48*, 1837–1855.

Nathan, T. R., E. C. Cordero, and L. Li (1994), Ozone heating and the destabilization of traveling waves during summer, *Geophys. Res. Lett.*, *21*, 1531–1534.

Nishii, K., and H. Nakamura (2004), Lower-stratospheric Rossby wave trains in the Southern Hemisphere: A case study for late winter of 1997, *Q. J. R. Meteorol. Soc.*, *130*(596), 325–345.

Peixoto, J. P., B. Saltzman, and S. Teweles (1964), Harmonic analysis of the topography along parallels of the earth, *J. Geophys. Res.*, *69*, 1501–1505.

Perlwitz, J., and N. Harnik (2003), Observational evidence of a stratospheric influence on the troposphere by planetary wave reflection, *J. Clim.*, *16*, 3011–3026.

Plumb, R. A., and K. Semeniuk (2003), Downward migration of extratropical zonal wind anomalies, *J. Geophys. Res.*, *108*(D7), 4223, doi:10.1029/2002JD002773.

Randel, W. J. (1987), Global Atmospheric Circulation Statistics 1000-1 mb, *NCAR Tech. Note NCAR/TN-295*, 245 pp., Natl. Center Atmos. Res., Boulder, Colo.

Randel, W. J. (1993), Global variations of zonal-mean ozone during stratospheric warming events, *J. Atmos. Sci.*, *50*, 3308–3321.

Salby, M. L., D. O'Sullivan, R. R. Garcia, and P. Callaghan (1990), Air motions accompanying the development of a planetary wave critical layer, *J. Atmos. Sci.*, *47*, 1179–1204.

Shindell, D. T., D. Rind, N. Balachandran, J. Lean, and P. Lonergan (1999), Solar cycle variability, ozone and climate, *Science*, *284*, 305–308.

World Meteorological Organization (2002), Scientific Assessment of Ozone Depletion: 2000, *Global Ozone Research and Monitoring Project No. 47*, World Meteorol. Org., Nairobi, Kenya.

Xu, J., A. K. Smith, and G. P. Brasseur (2001), Conditions for the photochemical destabilization of gravity waves in the mesopause region, *J. Atmos. Sol. Terr. Phys*, *63*, 1821–1829.

Zhu, X., and J. R. Holton (1986), Photochemical damping of inertio-gravity waves, *J. Atmos. Sci.*, *43*, 2578–2584.

E. C. Cordero, Department of Meteorology, San José State University, San José, CA 95192-0104, USA.

T. R. Nathan, Atmospheric Science Program, Department of Land, Air and Water Resources, University of California, One Shields Avenue, Davis, CA 95616-8627, USA. (trnathan@ucdavis.edu)